# Dynamics of Chloromethanes in Cryptophane-E Inclusion Complexes: A $^2$H Solid-State NMR and X-ray Diffraction Study

**Oleg Petrov,[†] Zdeněk Tošner,[‡] Ingeborg Csöregh, Jozef Kowalewski, and Dick Sandström***

*Department of Physical, Inorganic, and Structural Chemistry, Arrhenius Laboratory, Stockholm University, SE-106 91 Stockholm, Sweden*

*Received: November 8, 2004; In Final Form: April 1, 2005*

In this paper, we present a variable temperature $^2$H solid-state NMR investigation of cryptophane-E:chloroform and cryptophane-E:dichloromethane inclusion complexes. The $^2$H line shapes and nuclear spin relaxation rates were analyzed in terms of the distribution of C−D bond orientations and the time scale of the guest dynamics. It was found that encaged chloroform produces broad $^2$H spectra, and that its reorientation is relatively slow with a correlation time of ∼0.17 $\mu$s at 292 K. In contrast, the $^2$H line shapes of encaged dichloromethane are narrow and the motion of this guest molecule is fast with a correlation time of ∼1.4 ps at 283 K. The $^2$H NMR data were complemented by an X-ray diffraction study of the cryptophane-E:dichloromethane structure, which was utilized in the analysis of the NMR parameters.

## 1. Introduction

A vast number of synthetic host molecules able to recognize and bind small guest molecules can nowadays be found in the literature.[1,2] The selective capture of a neutral substrate by a molecular receptor is based on shape complementarity and the presence of noncovalent interactions. Understanding the intermolecular forces that govern the complexation in such supramolecular systems may provide a detailed picture of enzyme−substrate and antigen−antibody association and may be used to design artificial molecular devices and sensors.

Cryptophane-E (see Figure 1) is known as a host suitable for the inclusion complexation of small neutral guests of volumes up to ∼90 Å$^3$, and preferably those of tetrahedral structure.[1,3] The most stable complex is formed with chloroform ($CHCl_3$) as it fits well in terms of both size and the 3-fold symmetry of the host cavity. The complexation of $CHCl_3$ is driven by the enthalpically favorable formation of van der Waals bonds.[1,4] In contrast, the complex with the smaller guest dichloromethane ($CH_2Cl_2$) is substantially weaker, and the complexation is in this case entropy driven.[1,4] The X-ray structure of the cryptophane-E:$CHCl_3$ complex has been determined by Canceill et al.[4]

Previously, some of us investigated the dynamics of the above-mentioned complexes in tetrachloroethane solution by using nuclear magnetic resonance (NMR) spectroscopy.[5,6] For chloroform, no fast large-amplitude motion of the C−H bond inside the host cavity was observed, demonstrating a strong motional coupling between the guest and the host. The dynamics of dichloromethane, in contrast, was found to be only weakly coupled to the reorientation of the host. More recently, we also reported a preliminary study of the crystallized complexes by means of advanced $^{13}$C solid-state NMR experiments.[7] It was found that the guest molecules occupy two different sites in the crystal: one inside the cryptophane-E cavity and the other in interstitial positions. Measurements of site-resolved $^1$H−$^{13}$C through-space dipolar couplings confirmed the observations made in solution and suggested a similar behavior in the solid state.

The present work is a comprehensive $^2$H NMR study of the dynamics of the complexes in the solid state. We also report the X-ray structure of the cryptophane-E:$CH_2Cl_2$ system. Analysis of $^2$H NMR line shapes is a well-established technique for investigations of dynamical processes in solids.[8−12] The analysis consists of comparisons between the experimental line shapes and calculated counterparts assuming a particular model of the motion. This can provide information on the geometry of molecular bond motions, the bond orientation probabilities, and under favorable conditions, the correlation time $\tau_c$. In the fast motional regime, where the NMR line shape is independent of $\tau_c$, information on the geometry of the motion can be used to develop an orientation dependent correlation function, and $^2$H spin relaxation data can then be analyzed to determine the correlation times.[13] Deuterium NMR data are ideally suited to be combined with X-ray diffraction (XRD) measurements to obtain a plausible motional model.[14,15] This approach is especially rewarding for systems with many degrees of freedom, as is the case for the van der Waals complexes investigated here.

Two problems frequently encountered in $^2$H solid-state NMR of powders containing different $^2$H sites are spectral assignment and overlap. By combining the knowledge previously obtained from $^{13}$C magic-angle spinning (MAS) NMR experiments[7] with the present $^2$H NMR and XRD data, however, we have been able to obtain a detailed picture of the dynamical behavior of the cryptophane-E:chloromethane inclusion complexes.

## 2. Theory

This section briefly summarizes the theory used for analyzing our experimental $^2$H NMR data.

**2.1. Motional Effects on $^2$H Solid-State NMR Spectra.** The $^2$H quadrupolar coupling stems from the interaction between

* Corresponding author. Fax: +46-8-152187. E-mail: dick.sandstrom@physc.su.se.

[†] On leave from the Department of Physics, Kazan State Technological University, 420015 Kazan, Russian Federation.

[‡] On leave from the Department of Low-Temperature Physics, Faculty of Mathematics and Physics, Charles University, V Holešovičkách 2, CZ-180 00 Prague 8, Czech Republic.

10.1021/jp044884a CCC: $30.25 
Published on Web 05/03/2005

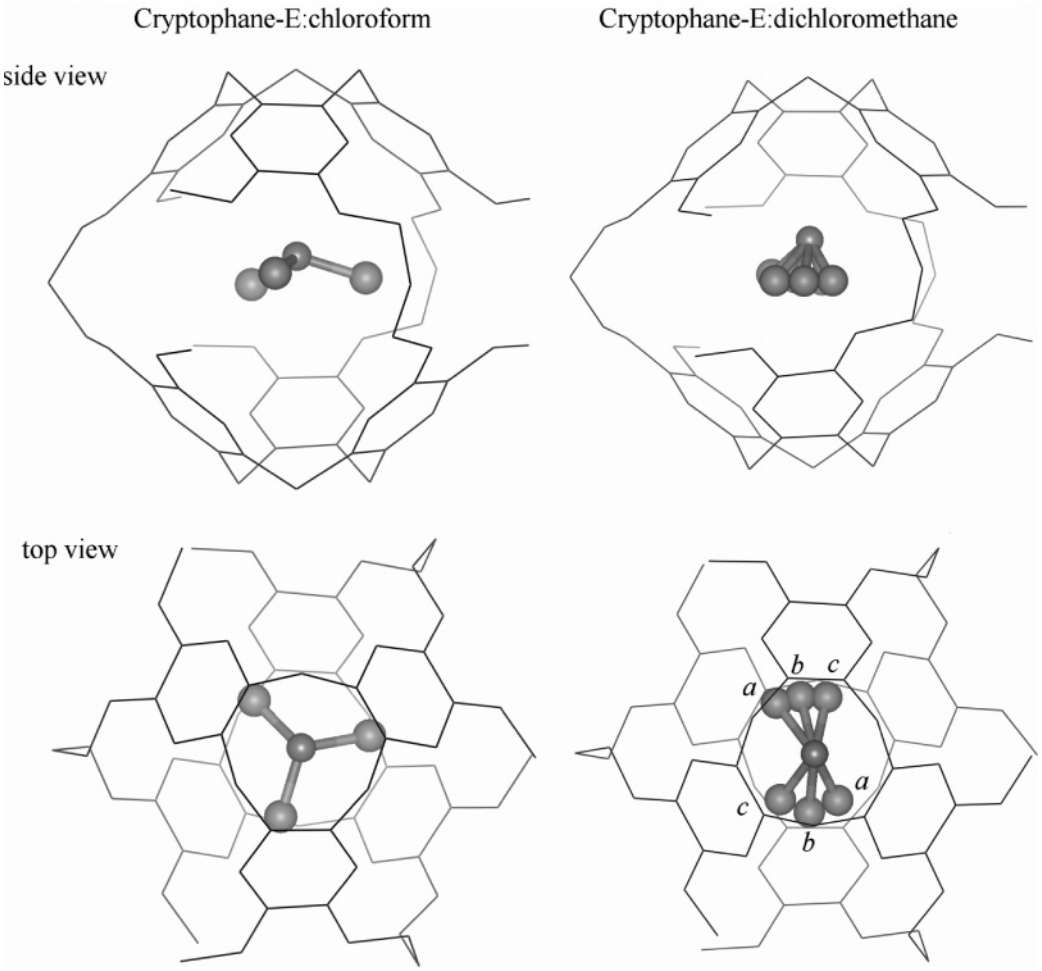


**Figure 1.** X-ray models of the inclusion complexes of cryptophane-E with chloroform (left) and dichloromethane (right). For simplicity, only guest sites above the equatorial plane of the host are shown. The letters *a*−*a*, *b*−*b*, and *c*−*c* in the lower right panel indicate Cl atoms of the three major dichloromethane positions. For additional crystallographic illustrations of the cryptophane-E:dichloromethane complex, see the Supporting Information.

the electric quadrupolar moment $eQ$ of the nucleus and the electric field gradient (EFG) tensor $\mathbf{V}$. This second-rank tensor is, in its principal axis system (PAS), defined by the magnitude $V_{ZZ}^{PAS} = eq$ and the asymmetry parameter $\eta = (V_{XX}^{PAS} - V_{YY}^{PAS})/V_{ZZ}^{PAS}$, where $0 \leq \eta \leq 1$. We use the convention $|V_{ZZ}^{PAS}| \geq |V_{YY}^{PAS}| \geq |V_{XX}^{PAS}|$. It is customary to define the strength of the $^2$H quadrupolar coupling in terms of the quadrupolar coupling constant $QCC = e^2qQ/h$ which, in frequency units, is ∼170 kHz for $^2$H nuclei in sp$^3$-hybridized C−D groups.[11]

The tensor nature of the quadrupolar interaction leads to an orientation dependence of the $^2$H NMR frequencies in the solid state. For powdered samples, where all molecular orientations are present, this dependence results in a $^2$H NMR spectrum spanning the range −3QCC/4 to +3QCC/4 in the absence of motion. In addition to QCC, the spectral line shape is also governed by the asymmetry parameter. A spectrum with $\eta = 0$ is often referred to as a $^2$H Pake pattern.[16]

In the presence of molecular motions, the C−D bond orientation varies with time and the $^2$H line shape generally changes as compared to the rigid lattice case. The changes become most pronounced if the reorientation rate is comparable to, or exceeds, QCC. In the fast motion limit, where the correlation time satisfies $\tau_c^{-1} >> 2\pi$QCC (or typically $\tau_c << 10^{-6}$ s), the $^2$H quadrupolar interaction is effectively averaged to give a residual EFG tensor $\langle\mathbf{V}\rangle$. Expressed in a static, crystal-fixed axis system (CAS), the elements of $\langle\mathbf{V}\rangle$ are, for a discrete motion, given by

$$\langle V_{ij}\rangle = \sum_{k=1}^{N} V_{ij}(\Omega_k)\, P(\Omega_k) \tag{1}$$

where $N$ is the number of sites, $\Omega_k = (\varphi, \theta, \psi)_k$ are the Euler angles specifying the orientation of PAS for site $k$ relative to CAS, and $P(\Omega_k)$ is the probability of site $k$. In the case of a continuous motion, the elements of $\langle\mathbf{V}\rangle$ can be written as

$$\langle V_{ij}\rangle = \int V_{ij}(\Omega)\, P(\Omega)\, \mathrm{d}\Omega \tag{2}$$

where $P(\Omega)$ is the distribution function. The resulting motionally averaged $^2$H NMR line shape can be described by a residual quadrupolar coupling constant $\langle$QCC$\rangle$ and asymmetry parameter $\langle\eta\rangle$. To calculate these quantities, the matrix $\langle\mathbf{V}\rangle$ has to be diagonalized, and the diagonal elements are arranged so that they satisfy the condition $|\langle V_{ZZ}\rangle| \geq |\langle V_{YY}\rangle| \geq |\langle V_{XX}\rangle|$. $\langle$QCC$\rangle$ and $\langle\eta\rangle$ can then be expressed in terms of these elements according to $\langle$QCC$\rangle$ = QCC$|\langle V_{ZZ}\rangle/V_{ZZ}|$ and $\langle\eta\rangle = (\langle V_{XX}\rangle - \langle V_{YY}\rangle)/\langle V_{ZZ}\rangle$. The reduction of the spectral splitting $\langle$QCC$\rangle$/QCC is often called the local order parameter. Equations 1 and 2 provide relationships between the $\langle$QCC$\rangle$ and $\langle\eta\rangle$ values and the geometry of the motion.

For discrete motions, irrespective of the motional time scale, the $^2$H line shape can be calculated by solving a set of exchange-

modified Bloch equations and several programs for this purpose have been reported.[9,17]

A rough estimate of the motional time scale can be obtained by studying the effect of varying the delay time $\tau$ in the quadrupolar echo pulse sequence $[(\pi/2)_x-\tau-(\pi/2)_{\pm y}-\tau-\text{acq}]$,[18] which is the standard technique to record $^2$H solid-state NMR spectra. In the fast motion limit, the line shape is independent of $\tau$. For motions in the intermediate regime with $\tau_c$ around $(2\pi\text{QCC})^{-1}$, however, losses of the echo intensity with increasing $\tau$ become frequency dependent, so that the spectrum visibly changes when $\tau$ is increased.[10]

**2.2. Deuterium Spin−Lattice Relaxation.** The general expression for the $^2$H spin−lattice relaxation rate is[13]

$$\frac{1}{T_1} = \frac{\omega_Q^{\,2}}{3}[J_1(\omega_0) + 4J_2(2\omega_0)] \tag{3}$$

where $\omega_Q = 3\pi\text{QCC}/2$, $\omega_0$ is the $^2$H resonance frequency, and $J_m(\omega_0)$ are the reduced spectral density functions defined by

$$J_m(\omega_0) = 2\int_0^\infty C_m(t)\cos(\omega_0 t)\,\mathrm{d}t \tag{4}$$

In eq 4, $C_m(t)$ are the autocorrelation functions for the spherical harmonics, $Y_{2,m}$, of the polar angles specifying the direction of PAS with respect to the static magnetic field direction. In solids, $C_m(t)$ are dependent on the orientation of the crystal frame with respect to the static field so that $C_m(t) = C_m(t;\alpha,\beta)$, where the polar angles $\alpha$ and $\beta$ specify the orientation of the magnetic field in CAS. This dependence results in $T_1$ anisotropy.[9,19] The time evolution of the total intensity, integrated over the entire line shape, in an inversion recovery (IR) relaxation experiment is thus in general multiexponential. However, because the $T_1$ values corresponding to different crystallite orientations are in many cases of comparable magnitude, a single-exponential relaxation is often observed. In such cases, powder averaged autocorrelation functions $\bar{C}_m(t)$ are associated with the apparent spin−lattice relaxation rate. In a variety of situations, $\bar{C}_m(t)$ can either be expressed in closed form[13,20] or calculated numerically[9] provided that the geometry of the motion is known.

Qualitatively, the motional regimes can be assessed from the temperature dependence of $T_1$, because plots of $T_1(1/T)$ and $T_1(\log \tau_c)$ are equivalent due to the Arrhenius behavior of $\tau_c(T)$. When $\tau_c$ satisfies $\omega_0^2\tau_c^2 << 1$ (the extreme narrowing regime), $T_1$ is a decreasing function of $\tau_c$. $T_1$ reaches its minimum when $\omega_0^2\tau_c^2 \approx 1$, and in the slow motion limit where $\omega_0^2\tau_c^2 >> 1$ holds, $T_1$ increases with $\tau_c$.

## 3. Materials and Methods

**3.1. Materials.** The inclusion complexes were crystallized from solutions of cryptophane-E in respective guests at near-critical concentrations by slow evaporation of the solvent. To prepare the cryptophane-E:chloroform-*d* complex for $^2$H NMR experiments, cryptophane-E ($C_{57}H_{60}O_{12}$, Acros Chemicals, 97%) was dissolved in neat chloroform-*d* ($CDCl_3$, Cambridge Isotope Laboratories, 99.8%) in a concentration of 38 mg/mL and left to evaporate in air at ambient temperature during 2 days. When the bulk solvent was no longer visible, the crystals were ground to a powder and left to dry for another 2 days under the same conditions. Finally, the powder was packed into a 5 mm screw-lid plastic container and sealed by Parafilm tape. The sample of the cryptophane-E:dichloromethane complex was prepared by dissolving cryptophane-E in a 1:3 mixture of dichloromethane-$^{13}$C ($^{13}CH_2Cl_2$, Cambridge Isotope Laboratories, 99%) and dichloromethane-$d_2$ ($CD_2Cl_2$, Cambridge Isotope Laboratories, 99.9%) in a concentration of 23 mg/mL and left to evaporate in air at ambient temperature during 2 days. After the bulk solvent had disappeared, the crystals were ground and packed into a 4 mm $ZrO_2$ rotor. No extra drying was applied to this sample because it was found to quickly deteriorate in open air. This cryptophane-E:dichloromethane sample was also used in our previous $^{13}$C solid-state NMR study.[7]

**TABLE 1: Encaged:Interstitial Guest Ratios in Single Crystal and Powder Samples of the Cryptophane-E:Chloromethane Inclusion Complexes**

| | guest | |
|---|---|---|
| method | $CHCl_3$ | $CH_2Cl_2$ |
| XRD (single crystal) | 1:0.2[a] | 1:2[b] |
| TGA (powder) | 1:0.84[b] | – |
| $^{13}$C MAS NMR (powder) | 1:0.87[c] | 1:1.5[c] |

[a] From ref 4 (crystal grown from a chloroform/ethanol solution). [b] This work. [c] From ref 7.

The powder samples were characterized by thermal gravimetric analysis (TGA) and/or $^{13}$C MAS NMR spectroscopy. The $^{13}$C MAS NMR spectra of both complexes exhibit well-resolved resonances from encaged and interstitial guests and are fully consistent with $^{13}$C solution spectra.[7] In the cryptophane-E:dichloromethane sample, chloroform-$^{13}$C was found as an impurity originating from $^{13}CH_2Cl_2$. Although its content in $^{13}CH_2Cl_2$ was only 1.3%, it rose to 13% of $^{13}$C-enriched guests in the final product due to cryptophane-E's selectivity for chloroform (note, however, that there was no chloroform-*d* in the sample). Ratios of encaged to interstitial guests were determined from single-pulse $^{13}$C MAS NMR spectra, as well as from TGA, and the values are given in Table 1 along with the corresponding single-crystal XRD data. The $^{13}$C MAS NMR spectra of the complexes can be found in the earlier work from our laboratory.[7]

**3.2. X-ray Diffraction Measurements.** Crystals for the XRD study of the cryptophane-E:dichloromethane complex were grown from neat $CH_2Cl_2$ solution by slow solvent evaporation. The selected single crystal, when removed from the solvent, was immediately covered with epoxy glue to prevent crystal deterioration during the diffraction experiment. X-ray intensity data were collected at low temperature (123 K) using a STOE imaging plate detection system (IPDS) instrument equipped with an Oxford cryostream cooler. The net intensities were corrected for Lorentz, polarization, and absorption effects.[21] Application of direct methods with SHELXS[22] yielded reasonable positions of the C and O atoms of the cryptophane-E skeleton, and also some additional electron density peaks. The solution of the structure from this starting point was, however, not straightforward. The proximity and overlap of the partially occupied $CH_2Cl_2$ sites enhanced the difficulty to realize and refine the disorder models of the guest entities. The site occupation factors (sofs) and the atomic displacement parameters of the guest C and Cl disorder sites were refined in consecutive least-squares calculations with SHELXL-97.[23] In the last stage of the refinement procedure, the C and O atoms of the cryptophane-E host, and the C and Cl guest disorder sites with sof > 0.10 were refined together with their anisotropic displacement parameters, whereas the four Cl positions with sof < 0.10 were treated isotropically. Isotropic displacement parameters were refined also for the cryptophane-E hydrogen atoms, which were located to positions calculated using geometric evidence.[23] Neither disorder sites with sof < 0.05 nor partially occupied H sites were included in the final structure model. Moreover, the disordered guests, particularly the space filling ones between the 1:1 complex units (see below), had to be refined with simple

**TABLE 2: Summary of Crystal Data, Experimental Parameters, and Selected Details of the Refinement Calculations for the XRD Analysis of the Cryptophane-E:$CH_2Cl_2$ Complex**

| | |
|---|---|
| CCDC deposition number[a] | 247940 |
| empirical formula (sum) | $C_{60}\ H_{66}\ Cl_6\ O_{12}$ |
| empirical formula (moiety) | $C_{57}\ H_{60}\ O_{12} \times 3(CH_2Cl_2)$ |
| formula weight | 1191.83 |
| temperature (K) | 123(2) |
| wavelength (Å) | Mo Kα/0.71073 |
| crystal system | Monoclinic |
| space group (no.) | $P2_1/n$ (no. 14) |
| $a$ (Å) | 12.7580(10) |
| $b$ (Å) | 12.2410(10) |
| $c$ (Å) | 38.158(4) |
| α (deg) | 90.0 |
| $\beta$ (deg) | 95.711(12) |
| $\gamma$ (deg) | 90.0 |
| $V$ (Å$^3$) | 5229.6(9) |
| Z | 4 |
| $D_c$ (g cm$^{-3}$) | 1.335 |
| $\mu$ (mm$^{-1}$) | 0.350 |
| $F$(000) | 2496 |
| crystal size (mm) | 0.15 × 0.22 × 0.30 |
| $\theta$ range for data collection (deg) | 2.05 to 26.10 |
| index ranges | $-15 \le h \le 15$<br>$-15 \le k \le 14$<br>$-31 \le l \le 31$ |
| no. of reflections collected | 29349 |
| no. of unique reflections | 8182 |
| absorption correction,[b] $T_{max}/T_{mis}$ | numerical,0.95/0.84 |
| refinement method[c] | full-matrix least-squares on $F^2$ |
| no. of parameters refined | 1002 |
| $wR_2$[d] [for all unique $F^2$] | 0.166 |
| $R_1$ [for $F$ with $F > 4\sigma(F)$] | 0.056 |
| no. of $F$ with $F > 4\sigma(F)$ | 4919 |
| $S$ (goodness-of-fit on $F^2$) | 0.932 |
| final shift/esd, mean/max | 0.007/0.133 |
| final $\Delta\rho_{max}$, $\Delta\rho_{min}$ (e$^-$ Å$^{-3}$) | +0.32, −0.38 |

[a] Crystallographic data have been deposited with the Cambridge Crystallographic Data Centre as supplementary publication no. 247940. Copies of the data can be obtained free of charge upon application to CCDC, 12 Union Road, Cambridge CB2 1EZ, U.K. (e-mail: deposit@ccdc.cam.ac.uk). [b] Absorption correction was carried out using the programs X-shape and X-red.[21] [c] Refinement with SHELXL-97.[23] [d] The weights of the $F^2$ values were calculated as $[\sigma^2(F^2) + (c_1P)^2 + c_2P]^{-1}$, where $P = (F_o^2 + 2F_c^2)/3$, and the constants, $c_1$ and $c_2$ had the values 0.011 and 0.0.[23]

distance constraints to yield acceptable geometry. Crystal data, and selected details of reduction and refinement calculations are summarized in Table 2.

**3.3. Deuterium NMR Measurements.** $^2$H solid-state NMR experiments were performed using a Chemagnetics Infinity-400 spectrometer operating at $\omega_0/2\pi = 61.4$ MHz (9.4 T). $^2$H spectra were recorded by employing the quadrupolar echo (QE) sequence[18] $[(\pi/2)_x-\tau-(\pi/2)_{\pm y}-\tau-\text{acq}]$ with a $\pi/2$ pulse duration of 1.4 $\mu$s, and a pulse spacing of $\tau = 40$ $\mu$s. The $^2$H spin−lattice relaxation rates were measured employing the nonselective inversion recovery experiment using quadrupolar echo detection (IRQE) $[\pi-t-(\pi/2)_x-\tau-(\pi/2)_{\pm y}-\tau-\text{acq}]$ with $\tau = 40$ $\mu$s. Due to long accumulation times (up to 1.5 h/spectrum), the number of relaxation delays $t$ was limited to ∼10. The number of scans varied between 800 and 9600, depending on the guest and type of experiment.

**3.4. Deuterium NMR Simulations.** $^2$H NMR line shapes were simulated using the program MXQET.[17] The simulations were performed using a rigid lattice quadrupolar coupling constant of QCC = 170 kHz and an asymmetry parameter $\eta = 0$ for $CDCl_3$, and QCC = 170 kHz and $\eta = 0.06$ for $CD_2Cl_2$.[24,25] The partially relaxed $^2$H NMR spectra obtained from the IRQE experiment were simulated by the program EXPRESS.[26,27] The data were fitted using the software Origin (Microcal Software, Inc.), which employs the Levenberg−Marquardt least-squares algorithm. Euler angles specifying the orientation of a guest molecule relative to CAS were calculated from the X-ray structure using a routine written by the authors. This routine calculates the Euler pseudo-active rotation matrix from the atom Cartesian coordinates of a molecule before and after rotation and then extracts the Euler angles from the matrix, using its explicit expression.[11]

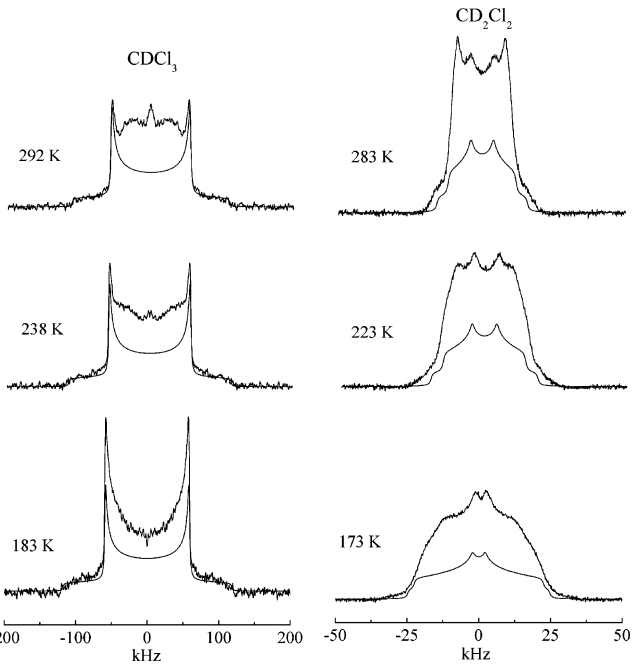


**Figure 2.** Variable temperature $^2$H solid-state NMR spectra of the inclusion complexes of cryptophane-E with $CDCl_3$ (left) and $CD_2Cl_2$ (right). The spectra in each column are normalized so that they have equal areas. The simulated lines show contributions from the encaged guests (see text for details). The difference in the frequency scale should be noticed.

## 4. Results

**4.1. Cryptophane-E:Chloroform Complex.** *4.1.1. X-ray Structure of the Complex.* We proceed in our work from the crystal structure of the cryptophane-E:$CHCl_3$ complex reported by Canceill et al.[4] In that study, it was found that the host molecule is almost spherical and exhibits nearly $D_3$ rotational symmetry. The asymmetric unit of the crystal consists of one host molecule, one guest encaged inside the host cavity, and interstitial $CHCl_3$ in a nonstoichiometric ratio of 1:0.2. Encaged chloroform has two almost equivalent orientations relative to the pseudo-$C_3$ axis (i.e., the axis connecting the centers of the cyclotriveratrylene units of the host), in which the Cl atoms occupy the equatorial plane of the host, and its C−H bond points along the pseudo-$C_3$ axis (see Figure 1, left panels). Herein, we assume that the structure shown in Figure 1 also holds for our system, although the sample we studied had a different ratio of encaged to interstitial guests (cf. Table 1).

*4.1.2. Deuterium NMR Spectra.* Figure 2 (left panels) presents a series of variable temperature $^2$H NMR spectra of $CDCl_3$. It is evident, especially at elevated temperatures, that the spectra consist of at least two components, which obviously originate from encaged and interstitial guest molecules. We assign the broader component, having a characteristic Pake-type shape, to encaged $CDCl_3$, and the relatively featureless inner compo-

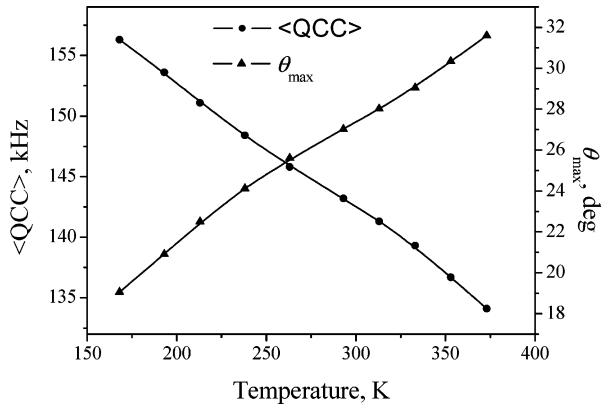


**Figure 3.** Temperature dependence of the residual quadrupolar coupling constant ⟨QCC⟩ for encaged $CDCl_3$. Half-angles $\theta_{max}$ calculated from ⟨QCC⟩ assuming diffusion in a cone are also shown.

nent to interstitial $CDCl_3$. This assignment is based on our previous measurements of site-resolved $^1H-^{13}C$ dipolar couplings, where interstitial chloroform was found to produce narrower and more featureless dipolar spectra as compared to those originating from encaged $CHCl_3$.[7] No significant line shape changes were observed for $^2H$ spectra obtained with longer QE delays indicating that the motion is fast compared to QCC.

Below, only the spectral component produced by encaged $CDCl_3$ will be examined thoroughly, because it is the dynamics of this guest that we focus on in this study. Fortunately, the sharp anisotropic features of this component enabled us to extract it from the $^2H$ NMR spectrum, provided that the fraction of encaged $CDCl_3$ is known. Simulations of these subspectra are included in Figure 2, and the values of ⟨QCC⟩ used in the line shape calculations are shown in Figure 3. From a comparison of ⟨QCC⟩ with the static QCC = 170 kHz, we find that the motional narrowing of the spectra does not exceed 21% (corresponding to local order parameters ≥0.79). An interesting feature is that the $^2H$ NMR line shapes indicate symmetric motion: the residual asymmetry parameter is zero over the entire temperature range investigated.

*4.1.3. Deuterium Spin−Lattice Relaxation.* Four IRQE experiments were performed in the temperature range 183−353 K. Figure 4 (left) and Figure 5 (left) show a representative series of partially relaxed $^2H$ spectra and the function $I(t)$ describing the recovery of the integrated intensity, respectively. We approximated $I(t)$ by two exponential functions: one for encaged and one for interstitial guests

$$I(t) = I_0[1 - (1 + \text{eff})\{p \exp(-t/T_1') + (1 - p) \exp(-t/T_1'')\}] \quad (5)$$

where $I_0$ is the equilibrium intensity, eff is the efficiency of the polarization inversion (eff = $|I(0)/I_0|$), and $p$ is the fraction of the encaged guest. The relaxation times $T_1'$ (describing encaged guests) and $T_1''$ (describing interstitial guests) are the only unknown parameters in eq 5, and their values can be readily obtained by fitting eq 5 to the experimental $I(t)$. To determine reliable initial $T_1$ values for the fitting procedure, we used the approach described in the Appendix. The best-fit curve for 292 K is shown in Figure 5 by a solid line, and the $^2H$ $T_1$ values are plotted in Figure 6 (left panel). The temperature dependence of $T_1$ indicates that the correlation time of encaged $CDCl_3$ satisfies the condition $\omega_0^2\tau_c^2 >> 1$ (i.e., motion outside of the extreme narrowing regime). Taking into account that the motion is fast on the $^2H$ quadrupolar interaction time scale, we can thus estimate the limits of $\tau_c$ as $10^{-9}$ s < $\tau_c$ < $10^{-6}$ s. Interstitial

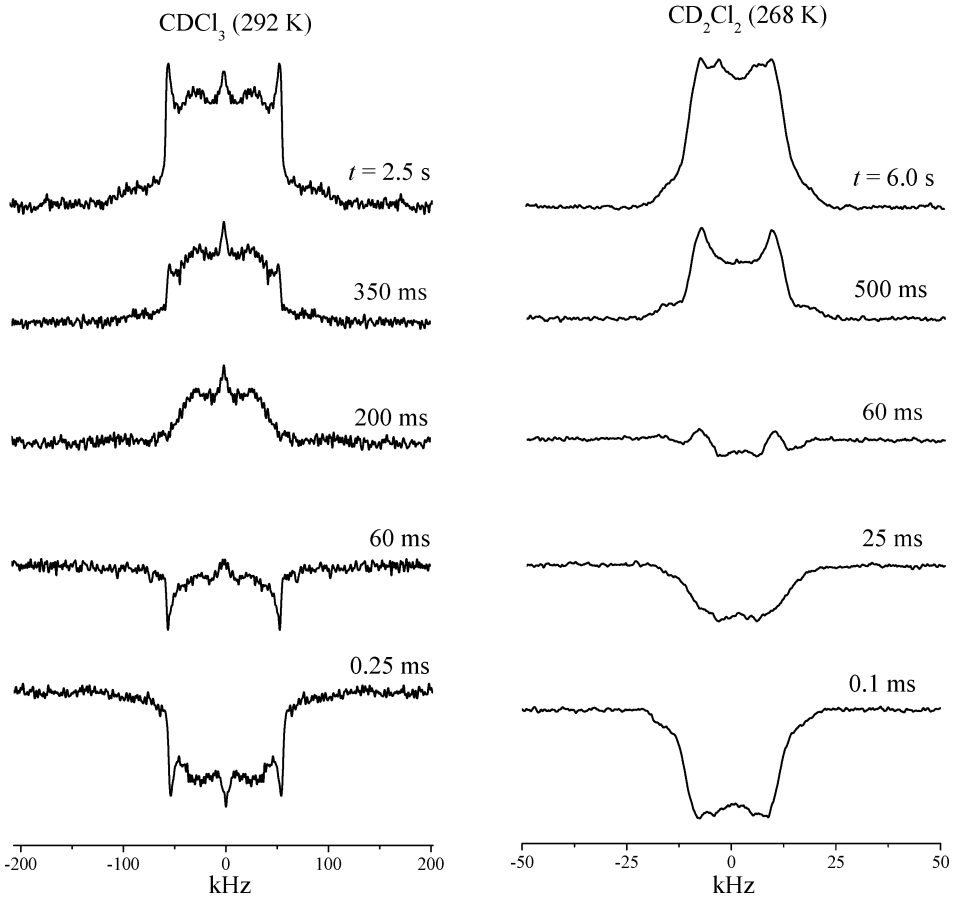


**Figure 4.** Representative partially relaxed $^2H$ NMR spectra of $CDCl_3$ (left) and $CD_2Cl_2$ (right) obtained by IRQE experiments.

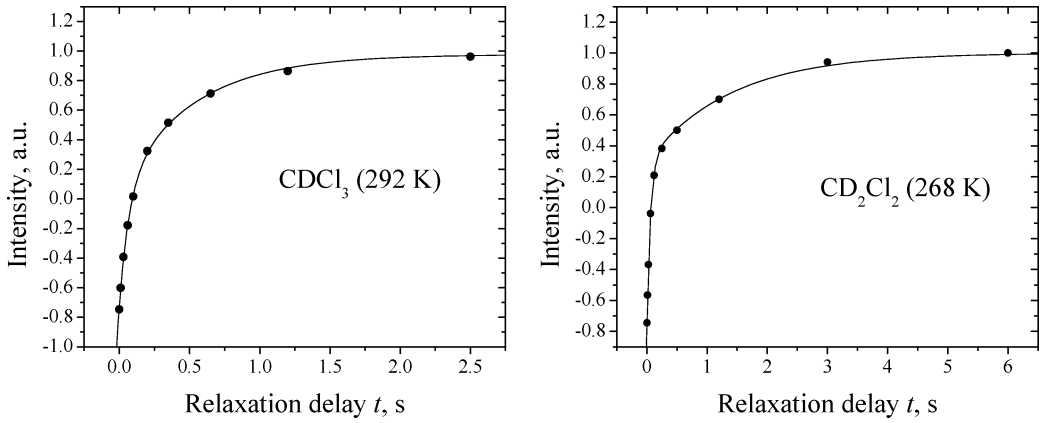


**Figure 5.** Recovery of the integrated intensities of $CDCl_3$ (left) and $CD_2Cl_2$ (right) corresponding to Figure 4. The solid lines show the best-fit curves to eq 5.

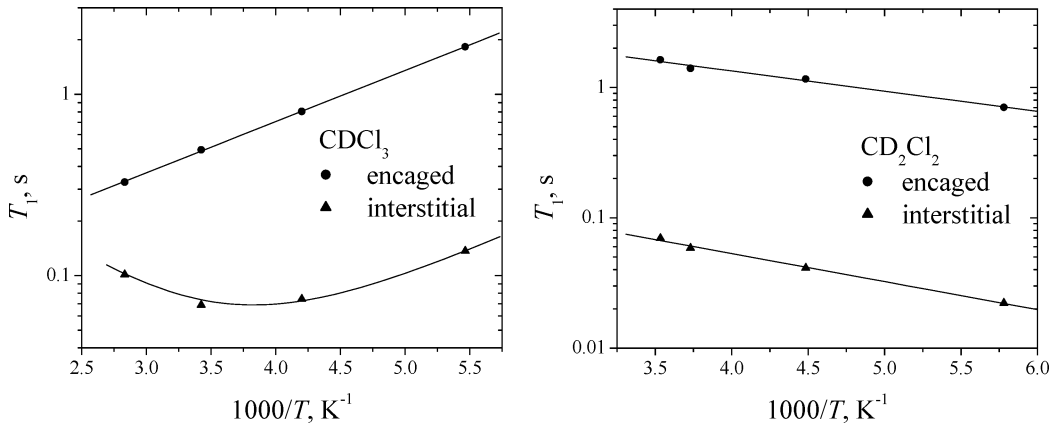


**Figure 6.** Temperature dependence of the $^2H$ $T_1$ relaxation times of $CDCl_3$ (left) and $CD_2Cl_2$ (right).

$CDCl_3$ seems to undergo a faster motion than the encaged one, with correlation times centered near $\omega_0^{-1}$ (i.e., near the $T_1$ minimum).

**4.2. Cryptophane-E:Dichloromethane Complex.** *4.2.1. X-ray Structure of the Complex.* Like in its complex with chloroform,[4] the solid cryptophane-E host displays a nearly $D_3$ rotational symmetry (see Figure 1, right panels) and forms inclusion crystals with monoclinic $P2_1/n$ space group symmetry (cf. Table 2). The unique unit contains one host molecule and approximately three dichloromethane guests. The partial occupancy and relatively high atomic displacement parameters indicate that the guests exhibit both static and dynamic disorder. One $CH_2Cl_2$ molecule resides within the cryptophane-E cavity, whereas the two others fill up the space between the 1:1 host−guest units. The model of the encaged guest includes two C and at least 11 Cl sites. The Cl positions, having variable site occupancies, are located close to the equatorial plane of the host, whereas the C sites are found near the pseudo-$C_3$ symmetry axis of the cryptophane-E molecule. One of these C positions has an occupation probability of 13%, whereas the other is 87% (henceforth referred to as the minor and major C site, respectively). Twenty-four additional electron density peaks could be resolved and interpreted as 17 Cl and seven C disorder sites, forming all together approximately two interstitial guests. The sofs for these guests refined to somewhat higher values for the C sites, and to lower values for the Cl sites than expected. Most likely, this is due to unresolved overlaps of the C and Cl guest sites.

Inspection of the intermolecular contact distances indicates only weak van der Waals forces between cryptophane-E and the $CH_2Cl_2$ molecules. The shortest approach, involving one of the host oxygens and one of the Cl disorder sites of the encaged guest, is somewhat longer than the sum of the van der Waals radii of the connected atoms (i.e., O···Cl $\approx 3.2 \pm 0.2$ Å).[28,29] The weak host−guest interaction forces in combination with the relatively small size of the $CH_2Cl_2$ molecule (as compared to the available space both within the cryptophane-E cavity and between the 1:1 host−guest associates) appear to allow for disorder and mobility of the dichloromethane molecules even at low (123 K) temperatures.

Because only C and Cl atoms could be realized in the X-ray model of the guest entities, and due to the extended overlap of the various sites (particularly for the guest inside the cavity), additional considerations had to be taken into account to group individual atom sites to encaged guests: (i) the Cl−C−Cl bond angles are expected to be close to 110°, and (ii) the Cl substituents, attached to either the major or the minor C site, should have a total occupation probability close to that of the respective C site. The atom sites that best fitted these requirements were grouped, and the result is presented in Figure 1 (right panels). For simplicity, only the major C and Cl sites are shown. The H and Cl coordinates of the encaged guest, deduced on the basis of the above-mentioned considerations, were used to calculate the Euler angles $\Omega = (\varphi, \theta, \psi)$ specifying the orientation of the principal axis system of the EFG tensor with respect to CAS. The $Z$ axis of CAS was chosen to coincide with the pseudo-$C_3$ symmetry axis of the host, and PAS has its $Z$ axis directed along one of the two C−H bonds of the guest. The result of this calculation is summarized in Table 3. For the major sites, the guest has one of its C−H bonds tilted at $\theta = 42 \pm 5°$ away from the pseudo-$C_3$ axis (see Figure 7). The difference in the angle $\varphi$ for these sites is $\Delta\varphi = 28°$. For the

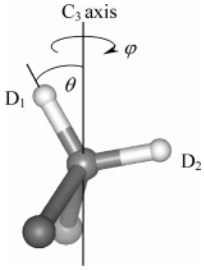


**Figure 7.** Illustration of the orientation of encaged dichloromethane in the crystal-fixed axis system (CAS). The *Z* axis of CAS is oriented along the pseudo-$C_3$ symmetry axis of the host.

**TABLE 3: Euler Angles (deg) Describing the Orientations of Encaged Dichloromethane Guests in a Crystal-Fixed Axis System (Definitions in Text), and the Corresponding Occupation Probabilities Estimated by XRD Analysis at 123 K**

| site | $\varphi$ | $\theta$ | $\psi$ | probability |
|---|---|---|---|---|
| 1 | 352 | 47 | 262 | |
| 2 | 324 | 41 | 266 | 0.87 (major) |
| 3 | 296 | 38 | 267 | |
| 4 | 32 | 199 | 266 | |
| 5 | 7 | 196 | 291 | 0.13 (minor) |
| 6 | 293 | 195 | 275 | |

minor sites, the tilt angle of the C−H bond is $\theta = 197 \pm 2°$ and $\Delta\varphi = 50 \pm 25°$. This rather complicated picture of the 1:1 host−guest unit is most likely due to a symmetry mismatch between the cryptophane-E host and $CH_2Cl_2$. Although only 11 Cl sites of the encaged guest were resolved with certainty, it was possible to obtain a complete set of Euler angles for six molecular sites by assuming that the missing twelfth Cl position should give the same tilt angle $\theta$ as the rest of minor molecular sites.

*4.2.2. Deuterium NMR Spectra and Spin−Lattice Relaxation.* Figure 2 (right panels) shows $^2$H NMR spectra of the cryptophane-E:$CD_2Cl_2$ complex as a function of temperature. As for $CDCl_3$, $CD_2Cl_2$ exhibits a two-component spectral pattern due to the presence of both encaged and interstitial guest molecules. The existence of two components is also apparent from the partially relaxed $^2$H spectra in which the inner part is seen to relax significantly slower than the outer one (cf. Figure 4, right).

The right panel in Figure 5 presents the recovery of the integral intensity of the $^2$H IRQE spectra obtained at 268 K, and the best-fit values of $T_1$ versus temperature are plotted in Figure 6. The temperature dependence of $T_1$ for both $CD_2Cl_2$ components corresponds to the extreme narrowing limit (i.e., $\omega_0^2\tau_c^2 << 1$, or $\tau_c << 10^{-9}$ s). To assign the two components, we have again made use of results from our previous $^{13}$C solid-state NMR study.[7] The $^{13}$C resonance from encaged dichloromethane was found to relax much slower than the interstitial counterpart. The $^{13}$C spin−lattice relaxation is mainly governed by the $^1$H−$^{13}$C dipolar interaction. In the extreme narrowing limit, both dipolar and quadrupolar $T_1$ values are inversely proportional to $\tau_c$. Thus, we attribute the inner, slowly relaxing component of the $^2$H NMR spectrum to encaged $CD_2Cl_2$, and the outer, having a faster relaxation, to interstitial $CD_2Cl_2$ molecules.[30] In the extreme narrowing limit, the relation $T_1^{\text{encaged}} > T_1^{\text{interstitial}}$ suggests that encaged $CD_2Cl_2$ move faster than the interstitial one, i.e., that $\tau_c^{\text{encaged}} < \tau_c^{\text{interstitial}}$ holds.

The large difference of the $^2$H $T_1$ values of encaged and interstitial $CD_2Cl_2$ enabled us to efficiently suppress the component produced by encaged $CD_2Cl_2$ by setting the relaxation delay $t$ in the IRQE experiment to its null-point, $t_{\text{null}} = T_1^{\text{encaged}} \times \ln(1 + \text{eff})$, which is long enough for the interstitial guest component to fully recover. By subtracting the latter from the fully relaxed $^2$H NMR spectrum, we could thus extract the encaged guest component with minor distortions (see Figure 8, left panels). To check the accuracy of this procedure, we calculated the fraction of the component produced by encaged $CD_2Cl_2$ and, depending on temperature, it was found to vary between 42% and 51%. These values are in reasonable agreement with the value of 40% predicted by the $^{13}$C MAS NMR data (cf. Table 1).

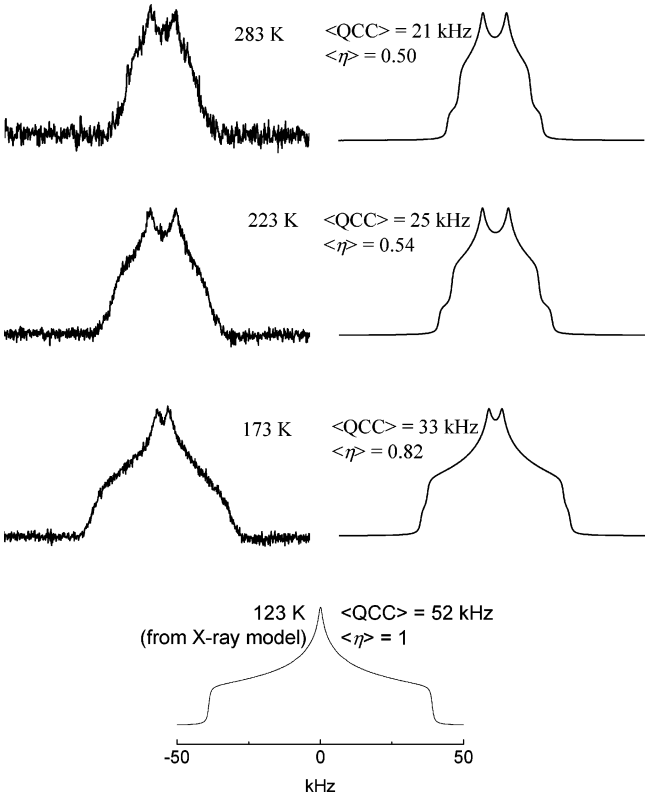


**Figure 8.** Variable temperature contributions from encaged $CD_2Cl_2$ to the $^2$H NMR spectra (left), and best-fit simulations (right). The $^2$H quadrupolar parameters used in the line shape simulations are indicated. The $^2$H NMR spectrum of $CD_2Cl_2$ calculated directly from the X-ray model obtained at 123 K is also shown (bottom).

The right panels in Figure 8 show simulated $^2$H spectra of encaged $CD_2Cl_2$ along with the values of the residual $^2$H quadrupolar interaction parameters used in the simulations (these spectra are also included in Figure 2, right panels). Note that the motion of $CD_2Cl_2$ averages QCC down to 12% of the rigid lattice value, which should be compared to 85% for $CDCl_3$ within the same temperature range. In addition, the $CD_2Cl_2$ spectra exhibit significant asymmetry with $\langle\eta\rangle$ values between 0.50 and 0.82 (remember that $\langle\eta\rangle$ was identically zero for $CDCl_3$). Below, we discuss these spectral features of the complexed guests in terms of various motional models.

## 5. Discussion

**5.1. Cryptophane-E:Chloroform Complex.** The broad and symmetric $^2$H NMR spectra of encaged $CDCl_3$ (cf. Figure 2, left panels) indicate that its C−D bond orientations are distributed with equal probability within a rather small angle relative to an average crystal-fixed direction. According to the X-ray structure of the complex, the pseudo-$C_3$ axis of cryptophane-E is most likely this direction (see Figure 1, left panels).

There are several models that may be suitable to describe the motion of encaged $CDCl_3$. We started with the diffusion in

**TABLE 4: Effective Correlation Times $\tau_c$ (in $\mu$s) of Encaged $CDCl_3$ Calculated Assuming Diffusion and 19-Site Jumps in a Cone**

| | motional model | |
|---|---|---|
| *T*, K | diffusion in a cone | 19-site jumps[a] |
| 183 | 0.41 | 0.35 |
| 238 | 0.22 | 0.22 |
| 292 | 0.17 | 0.16 |
| 353 | 0.15 | 0.14 |

[a] From simulations of the IRQE experiments.

the cone approach in which the C−D bond diffuses around the pseudo-$C_3$ axis in the angular region $0 \le \theta \le \theta_{max}$ and $0 \le \varphi \le 2\pi$. For this model, the distribution function in eq 2 is given by $P(\theta) = (1 - \cos \theta_{max})^{-1}$, which results in a reduction of the $^2$H quadrupolar splitting of

$$\langle QCC \rangle / QCC = \cos \theta_{max} (1 + \cos \theta_{max})/2 \qquad (6)$$

By substituting the experimentally obtained values of $\langle QCC \rangle$ into eq 6, we find that the half-angle of the cone $\theta_{max}$ varies between 19° at 168 K and 31° at 373 K (see Figure 3). These values, in combination with the relaxation data, can be used to estimate the effective correlation times. The approximate expressions for the autocorrelation functions derived by Lipari and Szabo[20,31] yield, after powder averaging,[13] the $\tau_c$ values listed in Table 4. All correlation times are found to be $<10^{-6}$ s, which is consistent with the results discussed in section 4.1.3.

The experimental $^2$H NMR spectra and spin−lattice relaxation rates were also analyzed using other motional models for encaged $CDCl_3$, and the general finding was that they produced $\tau_c$ values very similar to the ones listed in Table 4. For instance, the diffusion on the cone and three-site jump models result in correlation times that deviate <30% from the $\tau_c$ values obtained by assuming diffusion in a cone. The estimated correlation times are not very far from the inverse of the quadrupolar coupling constant $(2\pi QCC)^{-1} \approx 1$ $\mu$s. It should thus be possible to see some effects on the $^2$H line shape of $CDCl_3$ when $\tau$ is varied in the QE pulse sequence. Numerical simulations show, however, that the spectral changes are minor and probably unnoticeable in the experimental $^2$H spectra that consist of two components.

To conclude the discussion of the reorientational dynamics of encaged $CDCl_3$, we simulated the line shapes and IRQE experiments using a 19-site jump model in which the C−D bond undergoes nearest-neighbor jumps over a surface of a spherical segment. This closely spaced grid approach has previously been employed as an approximate model for diffusion in a cone.[17,32] The axially symmetric distribution of Euler angles describing the orientations of the C−D vector follows the scheme by Ronemus et al.[32] Partially relaxed $^2$H spectra were calculated for 17 relaxation delays and integrated over the entire $^2$H powder pattern. The recovery of the integrated intensity was fitted to a single-exponential function to extract the powder averaged $T_1$. The jump rates were varied until $T_1$ matched the experimental values, and the corresponding $\tau_c$ values are in good agreement with those obtained by the direct calculations discussed above (cf. Table 4). Figure 9 (left) presents examples of partially relaxed $^2$H NMR spectra of encaged $CDCl_3$ simulated with a correlation time of 0.16 $\mu$s (corresponding to $T = 292$ K).

In our previous paper,[7] we compared effective $^1$H−$^{13}$C dipolar couplings measured directly by $^{13}$C solid-state NMR with those obtained indirectly by means of $^{13}$C spin relaxation in solution. In the present work, we have estimated motionally averaged $^2$H quadrupolar couplings $\langle QCC \rangle$ of the deuterated guests. Because PAS of the $^2$H quadrupolar and $^1$H−$^{13}$C dipolar interaction tensors virtually coincide for the guest molecules, they are affected by motion in exactly the same way and it is possible to directly compare the averaging effects. The comparison is, however, somewhat complicated due to the fact that the static values of the $^1$H−$^{13}$C dipolar couplings for chloroform and dichloromethane are not precisely known. Assuming a rigid lattice spin−spin coupling strength $\delta_{CH}$ of 22.8 kHz (as was done in the $^{13}$C relaxation studies),[5,6] we obtain a ratio of the residual coupling $\langle \delta_{CH} \rangle$ and $\delta_{CH}$ of 0.82 and 0.84 for complexed chloroform in solution and solids, respectively. With a rigid lattice QCC = 170 kHz we find that, at similar temperatures, $\langle QCC \rangle / QCC$ is equal to 0.84. Thus, the local order parameter of the C−H/D bond is virtually equal in the liquid and solid state. The high value of the order parameter also shows that encaged chloroform behaves almost as an integral part of the cryptophane-E host. Raman microspectrometry studies[33] of this complex support these findings.

The Lipari−Szabo relaxation analysis of the complex in solution resulted in a correlation time of 22 ps for encaged chloroform ($T = 303$ K).[5] The present value obtained in the solid state is around 0.17 $\mu$s ($T = 292$ K). Such a large difference in correlation times may be explained by an increased rigidity of the cryptophane-E host cavity when going from the liquid to the solid phase. As being well integrated with the host, chloroform may experience this increased rigidity as changes in the reorientation potential barrier and/or in the chain fluctuation intensity of the host.

**5.2. Cryptophane-E:Dichloromethane Complex.** The X-ray model of this complex indicates the presence of six disordered sites of encaged dichloromethane, three on each side of the equatorial plane of the host. At the same time, the $^2$H solid-state NMR spectra unequivocally show motional effects of the encaged guest. Thus, we assume in what follows that the motion can be described as jumps between the six sites found by XRD.

Although $^2$H labeled dichloromethane has two deuterons, they clearly produce a $^2$H spectrum with a single anisotropic pattern under the motion (see Figure 8). This means that the two C−D bonds sample an equivalent set of orientations. This is possible, for example, if the two deuterons interchange when moving and that the interchange rate is fast on the $^2$H NMR time scale. Such a situation is analogous to a motion of a single C−D bond but moving through twice as many sites.

By assuming that the C−D bond can jump from one orientation to any other, we have simulated the $^2$H NMR line shape from the individual sites and their occupation probabilities listed in Table 3 (12 sites for one hypothetical C−D vector). The result is shown in Figure 8 (bottom panel). This may be considered a hypothetical $^2$H spectrum of encaged $CD_2Cl_2$ at $T = 123$ K resulting directly from the X-ray structure. To adapt this model to the experimental spectra, which were recorded at higher temperatures, simplifying assumptions are needed. We started by assuming that the probabilities and $\Delta\varphi$ for the minor and major C sites are equal at elevated temperatures, following the 2-fold symmetry of the host.[34] This assumption reduces the number of $^2$H sites for the NMR line shape simulation from 12 to 6, due to the invariance of the NMR spectrum under a $C_2$ transformation. Thus, we obtain a simplified six-site jump model in which $\theta$ and $\Delta\varphi$ are the only variable parameters (the angle $\psi$ was set to 270°). Table 5 shows the values of $\theta$ and $\Delta\varphi$ that fit the experimental $^2$H line shapes the best.

Deriving an explicit expression for the $^2$H $T_1$ relaxation rate for the six-site jump model becomes rather complicated. Therefore, we chose to analyze the relaxation data by performing

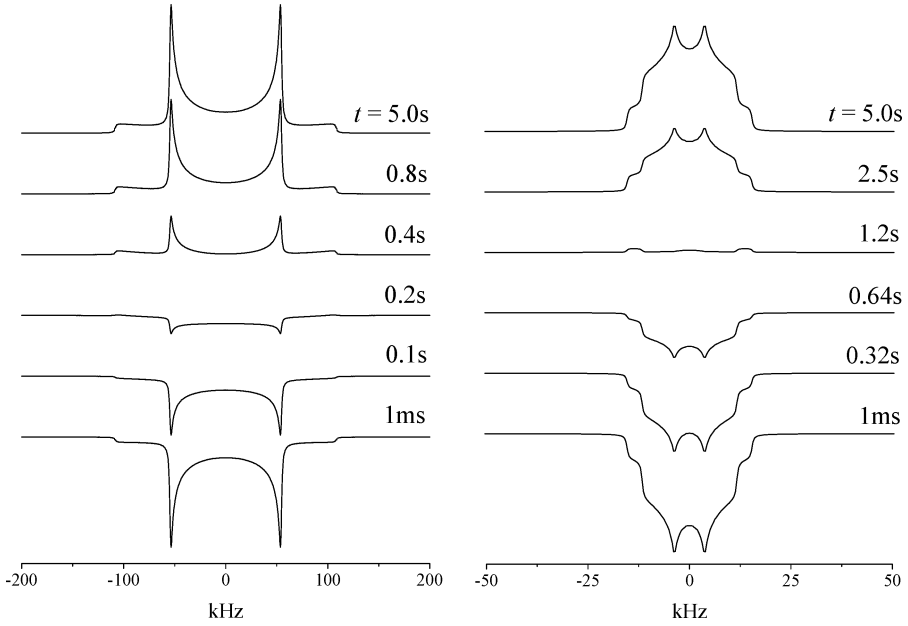


**Figure 9.** Representative partially relaxed $^2$H NMR spectra of encaged $CDCl_3$ (left) and $CD_2Cl_2$ (right) simulated assuming: (i) a 19-site jump model with $\theta_{max} = 22°$ and $\tau_c = 0.16$ $\mu$s for $CDCl_3$; (ii) a six-site jump model with $\theta = 48°$, $\Delta\varphi = 51°$, and $\tau_c = 1.4$ ps for $CD_2Cl_2$.

**TABLE 5: Temperature Dependence of Experimental ⟨QCC⟩ and ⟨$\eta$⟩ Values for Encaged $CD_2Cl_2$, and the Corresponding Parameters Assuming a Six-site Jump Model**

| $T$, K | ⟨QCC⟩, kHz | ⟨$\eta$⟩ | $\theta$, deg | $\Delta\varphi$, deg | $\tau_c$, ps[a] |
|---|---|---|---|---|---|
| 173 | 33 | 0.82 | | 43.5 | 3.6 |
| 223 | 25 | 0.54 | 48 | 48.0 | 2.1 |
| 283 | 21 | 0.50 | | 51.0 | 1.4 |

[a] $\tau_c = 1/(6k)$ where $k$ is the jump rate.

numerical simulations of the IRQE experiments in which $\theta$ and $\Delta\varphi$ were the input parameters in EXPRESS. Partially relaxed $^2$H spectra for 17 relaxation delays were simulated, and the jump rate was varied to fit the experimental $T_1$ values (an example is shown in Figure 9, right). The corresponding effective correlation times are given in Table 5.

We also analyzed the experimental spectra and relaxation data using other related motional models for encaged $CD_2Cl_2$ (for instance, by relaxing the assumption about a 2-fold symmetry of the host), and the general finding was that they produced correlation times very similar to the ones listed in Table 5 (not shown). It should be noted, however, that a simple two-site jump model was not able to reproduce the $^2$H line shapes.

Finally, we compare the motional averaging effects on the dipolar and quadrupolar interactions, and the correlation times for encaged dichloromethane. The $^{13}$C NMR studies reported previously[6,7] show that the $\langle\delta_{CH}\rangle/\delta_{CH}$ ratio is 0.14 and 0.15 in the liquid and solid state, respectively. In the present work, ⟨QCC⟩/QCC was found to be 0.12. The six-site jump model developed for encaged $CD_2Cl_2$ in the solid state gives nearly the same correlation time (1.4 ps at 283 K) as the one resulting from the Lipari−Szabo analysis of the complex in solution (1.8 ps at 273 K).[6] The agreement between the data sets indicates that the dynamics of the C−H/D vector in encaged dichloromethane is rather insensitive to the aggregation state of the system. The low values of $\langle\delta_{CH}\rangle/\delta_{CH}$ and ⟨QCC⟩/QCC also indicate that dichloromethane exhibits a much looser association with cryptophane-E as compared to chloroform.

## 6. Conclusions

We have in this paper presented a comprehensive $^2$H solid-state NMR and X-ray diffraction study of cryptophane-E: chloroform and cryptophane-E:dichloromethane inclusion complexes. Whereas diffraction experiments are particularly suited for determining the solid-state structure, $^2$H NMR spectroscopy more directly addresses dynamically disordered solids in terms of the distribution of C−D bond orientations and the time scale of the dynamics. The main conclusions of our study may be summarized as follows:

(i) The angular fluctuations of the C−D bond in encaged chloroform are very restricted, which agrees with previous NMR results obtained in the liquid state.[5,7] By assuming diffusion in a cone, we found a cone half-angle of 27° at 292 K. The correlation time for encaged chloroform in the solid state (∼0.17 $\mu$s at 292 K) is almost 4 orders of magnitude longer as compared to the value in solution.[5]

(ii) Encaged dichloromethane, in contrast, produces rather narrow $^2$H spectra, indicating a much looser association with the cryptophane-E host as compared to chloroform. This is, again, in agreement with solution NMR data.[6,7] On the basis of the X-ray structure of this complex, we showed that the motion of encaged dichloromethane can be modeled as jumps between six intracavity sites. Analysis of $^2$H $T_1$ relaxation using this model gives a correlation time of ∼1.4 ps at 283 K, which is very similar to the liquid-state value.[6]

The difference in dynamics of the two encaged chloromethane guests may be rationalized by considering their van der Waals sizes: dichloromethane is ∼20% smaller than chloroform and thus has more space to move in. Another possible explanation can be sought in the symmetry of the host and the guests and its effect on the host−guest potential: the matching 3-fold symmetry of chloroform and cryptophane-E can perhaps result in a relatively high barrier for the reorientation of encaged chloroform.

**Acknowledgment.** This work was supported by the Swedish Research Council, the Swedish Institute, the Magn. Bergvall Foundation, the Foundation of Lars Hierta's Memory, and the Carl Trygger Foundation. We thank Dr. K. Jansson for the TGA measurements. We are also grateful to Dr. G. Hoatson, Dr. R. L. Vold, and Dr. K. Müller for letting us use their $^2$H NMR simulation programs.

## Appendix

For systems producing two spectral components whose spin relaxation follows eq 5, the individual $T_1$ values can be obtained from the experimental function $I(t)$ by solving the coupled equations for the arithmetic and harmonic means of the $T_1$ values. Let us define a relaxation function $\Phi(t)$ according to

$$\Phi(t) = [I_0 - I(t)]/[I_0 + |I(0)|] = p\exp(-t/T_1') + (1-p)\exp(-t/T_1'') \quad \text{(A.1)}$$

which decreases from unity to zero. Integration of $\Phi(t)$ yields the arithmetic mean $\langle T_1 \rangle$

$$\langle T_1 \rangle = \int_0^\infty \Phi(t)\,\mathrm{d}t = pT_1' + (1-p)T_1'' \quad \text{(A.2)}$$

whereas the time derivative of $\Phi(t)$ at $t \rightarrow 0$ results in the harmonic mean $\langle T_1^{-1} \rangle$

$$\langle T_1^{-1} \rangle = -\lim_{t\to 0}\frac{\mathrm{d}\Phi}{\mathrm{d}t} = \frac{p}{T_1'} + \frac{1-p}{T_1''} \quad \text{(A.3)}$$

Provided that $p$ is known, the $T_1$ values can be determined from the area and initial slope of $\Phi(t)$ by solving the coupled eqs A.2 and A.3. This leads to a quadratic equation for $T_1'$

$$aT_1'^2 + bT_1' + c = 0 \quad \text{(A.4)}$$

where

$$a = p\langle T_1^{-1} \rangle \quad \text{(A.5)}$$

$$b = 1 - 2p - \langle T_1 \rangle \langle T_1^{-1} \rangle \quad \text{(A.6)}$$

$$c = p\langle T_1 \rangle \quad \text{(A.7)}$$

Because $a$, $c > 0$ and

$$b = -2p^2 - \frac{p(1-p)(T_1'^2 + T_1''^2)}{T_1'T_1''} < 0$$

eq A.4 has always one positive and one negative root, and only the former is physically correct.

**Supporting Information Available:** Additional crystallographic illustrations of the cryptophane-E:dichloromethane complex. This material is available free of charge via the Internet at http://pubs.acs.org.

## References and Notes


(1) Steed, J. W.; Atwood, J. L. *Supramolecular Chemistry*; John Wiley & Sons: Chichester, U.K., 2000.
(2) Bishop, R. *Chem. Soc. Rev.* **1996**, *25*, 311.
(3) Collet, A. *Tetrahedron* **1987**, *43*, 5725.
(4) Canceill, J.; Cesario, M.; Collet, A.; Guilhem, J.; Lacombe, L.; Lozach, B.; Pascard, C. *Angew. Chem., Int. Ed. Engl.* **1989**, *28*, 1246.
(5) Lang, J.; Dechter, J. J.; Effemey, M.; Kowalewski, J. *J. Am. Chem. Soc.* **2001**, *123*, 7852.
(6) Tošner, Z.; Lang, J.; Sandström, D.; Petrov, O.; Kowalewski, J. *J. Phys. Chem. A* **2002**, *106*, 8870.
(7) Tošner, Z.; Petrov, O.; Dvinskikh, S. V.; Kowalewski, J.; Sandström, D. *Chem. Phys. Lett.* **2004**, *388*, 208.
(8) Spiess, H. W. *Adv. Polym. Sci.* **1985**, *66*, 23.
(9) Wittebort, R. J.; Olejniczak, E. T.; Griffin, R. G. *J. Chem. Phys.* **1987**, *86*, 5411.
(10) Vega, A. J.; Luz, Z. *J. Chem. Phys.* **1987**, *86*, 1803.
(11) Schmidt-Rohr, K.; Spiess, H. W. *Multidimensional Solid-State NMR and Polymers*; Academic Press: London, 1994.
(12) Sandström, D.; Nygren, M.; Zimmermann, H.; Maliniak, A. *J. Phys. Chem.* **1995**, *99*, 6661.
(13) Torchia, D. A.; Szabo, A. *J. Magn. Reson.* **1982**, *49*, 107.
(14) Brouwer, E. B.; Enright, G. D.; Ratcliffe, C. I.; Facey, G. A.; Ripmeester, J. A. *J. Phys. Chem. B* **1999**, *103*, 10604.
(15) Benevelli, F.; Bond, A.; Duer, M.; Klinowski, J. *Phys. Chem. Chem. Phys.* **2000**, *2*, 3977.
(16) Pake, G. E. *J. Chem. Phys.* **1948**, *16*, 327.
(17) Greenfield, M. S.; Ronemus, A. D.; Vold, R. L.; Vold, R. R.; Ellis, P. D.; Raidy, T. E. *J. Magn. Reson.* **1987**, *72*, 89.
(18) Davis, J. H.; Jeffrey, K. R.; Bloom, M.; Valic, M. I.; Higgs, T. P. *Chem. Phys. Lett.* **1976**, *42*, 390.
(19) Hoatson, G. L.; Vold, R. L. *NMR Basic Princ. Prog.* **1994**, *32*, 1.
(20) Lipari, G.; Szabo, A. *J. Chem. Phys.* **1981**, *75*, 2971.
(21) *X-shape and X-red*; Stoe&Cie GmbH: Darmstadt, 1997.
(22) Sheldrick, G. M. *Acta Crystallogr.* **1990**, *A46*, 467.
(23) Sheldrick, G. M. *SHELXL-97*; University of Göttingen: Göttingen, 1997.
(24) Ragle, J. L.; Sherk, K. L. *J. Chem. Phys.* **1969**, *50*, 3553.
(25) Minott, G. L.; Ragle, J. L. *J. Magn. Reson.* **1976**, *21*, 247.
(26) Hoatson, G. L.; Vold, R. L.; Tse, T. Y. *J. Chem. Phys.* **1994**, *100*, 4756.
(27) Vold, R. L.; Hoatson, G. L.; Tse, T. Y. *Chem. Phys. Lett.* **1996**, *263*, 271.
(28) Bondi, A. *Physical Properties of Molecular Crystals, Liquids, and Glasses*; John Wiley & Sons: New York, 1968.
(29) Nyburg, S. C.; Faerman, C. H. *Acta Crystallogr.* **1985**, *B41*, 274.
(30) The $^2$H solid-state NMR spectrum of the cryptophane-E:$CD_2Cl_2$ complex shown in our earlier work[6] appears to consist of only one component. This was a result of recording the spectrum under saturation conditions (too short delays between successive acquisitions), which effectively suppressed the slowly relaxing component.
(31) Lipari, G.; Szabo, A. *Biophys. J.* **1980**, *30*, 489.
(32) Ronemus, A. D.; Vold, R. R.; Vold, R. L. *J. Chem. Soc., Faraday Trans. 1* **1988**, *84*, 3761.
(33) Cavagnat, D.; Brotin, T.; Bruneel, J. L.; Dutasta, J. P.; Thozet, A.; Perrin, M.; Guillaume, F. *J. Phys. Chem. B* **2004**, *108*, 5572.
(34) The thermal evolution of the cryptophane-E:dichloromethane crystal may be similar to that of urea/thiourea channel inclusion compounds (see, e.g.: Hollingsworth; et al. *J. Am. Chem. Soc.* **1999**, *121*, 9732. Sidhu; et al., *J. Phys. Chem. B* **1997**, *101*, 9087). At low temperatures, lattice stress generates distortions of the urea/thiourea channels and the fractional populations of the various guest sites are unequal. At higher temperatures, however, the site populations tend to be more equal and the inclusion compounds shift toward the undistorted structure.